Appl Compos Mater (2015) 22:99–118
DOI 10.1007/s10443-014-9394-3

Mechanical Modelling of Pultrusion Process: 2D and 3D Numerical Approaches

Ismet Baran · Jesper H. Hattel · Remko Akkerman · Cem C. Tutum

Received: 21 March 2014 / Accepted: 7 April 2014 / Published online: 29 May 2014

Abstract The process induced variations such as residual stresses and distortions are a critical issue in pultrusion, since they affect the structural behavior as well as the mechanical properties and geometrical precision of the final product. In order to capture and investigate these variations, a mechanical analysis should be performed. In the present work, the two dimensional (2D) quasi-static plane strain mechanical model for the pultrusion of a thick square profile developed by the authors is further improved using generalized plane strain elements. In addition to that, a more advanced 3D thermo-chemical-mechanical analysis is carried out using 3D quadratic elements which is a novel application for the numerical modelling of the pultrusion process. It is found that the 2D mechanical models give relatively reasonable and accurate stress and displacement evolutions in the transverse direction as compared to the 3D model. Moreover, the generalized plane strain model predicts the longitudinal process induced stresses more similar to the ones calculated in the 3D model as compared with the plane strain model.

Keywords Pultrusion process · Finite element analysis · Residual/internal stress · Thermosetting resin

I. Baran (✉) · J. H. Hattel
Department of Mechanical Engineering, Technical University of Denmark, DK-2800, Kgs., Lyngby, Denmark
e-mail: isbar@mek.dtu.dk

R. Akkerman
Faculty of Engineering Technology, University of Twente, NL-7500AE, Enschede, The Netherlands

C. C. Tutum
Department of Electrical and Computer Engineering, Michigan State University, East Lansing, MI, USA

Nomenclature

α	Degree of cure
α_{C0}	Critical degree of cure at $T = 0$ K
α_{CT}	Constant used in the shift factor ($f(\alpha, T)$)
C	Diffusion constant
Cp_c	Specific heat of the composite
Cp_d	Specific heat of the die
E	Activation energy
E_r	Instantaneous resin modulus
E_r^0	Initial (uncured) resin modulus
E_r^∞	Fully cured resin modulus
$f(\alpha, T)$	Shift factor (from kinetics to diffusion region)
H_{tr}	Total heat of reaction
$k_{x_1,c}, k_{x_2,c}, k_{x_3,c}$	Thermal conductivities in the x_1-, x_2- and x_3-directions, respectively for the composite
$k_{x_1,d}, k_{x_2,d}, k_{x_3,d}$	Thermal conductivities in the x_1-, x_2- and x_3-directions, respectively for the die
λ	Constant used in the Di Benedetto equation
K_o	Pre-exponential constant
n	Order of the cure reaction (kinetic exponent)
q	Heat source (internal heat generation)
ρ_c	Density of the composite
ρ_d	Density of the die
ρ_r	Density of the resin
R	Universal gas constant
$R_r(\alpha, T)$	Reaction of cure
t	Time
T	Instantaneous temperature
T_g	Glass transition temperature
T_{g0}	Glass transition temperature of the uncured resin
$T_{g\infty}$	Glass transition temperature of the fully cured resin
T^*	Difference between the glass transition temperature (T_g) and the instantaneous temperature (T)
T_{C1}	Critical temperature at the onset of the glass transition
T_{C2}	Critical temperature at the completion of the glass transition
u	Pulling speed
V_f	Fiber volume fraction

1 Introduction

Pultrusion is a continuous and a cost effective composite manufacturing process in which constant cross sectional profiles are produced. While pultrusion machines vary in design, the process is basically the same. Creels of unidirectional (UD) roving provide longitudinal tensile strength in the length of the profile. On the other hand, rows of continuous filament mat (CFM), woven roving or stitched fabrics provide transverse strength across the width of the profile. All reinforcements are first fed through the pre-forming guiders which start shaping the fiber reinforcements into the finished product. These reinforcements are then

pulled into a resin bath being wetted out and subsequently entering the heating die. The heaters initiate the exothermic reaction process in which the resin is being cured. The solidified and cured profile is advanced via a pulling system to the cut-off saw where it is cut to its final length. A schematic view of the pultrusion process is given in Fig. 1.

The process induced variations such as residual stresses and distortions are a critical issue in composite manufacturing [1–6], since they affect the structural behaviour and geometrical precision of the final product. More specifically, the residual stresses can lead to cracking during curing [1]. In order to capture and investigate these variations, a mechanical analysis should be performed.

In literature, thermo-chemical characteristics of the pultrusion process has been investigated numerically and experimentally [7–18] in which the temperature and degree of cure distributions inside the heating die were predicted. All these contributions have only been dealing with thermal modelling in which the temperature of the composite initially is lagging behind the heaters temperature; nevertheless during the curing it exceeds the die temperature due to the internal heat generation of the resin [7]. For this purpose, well known numerical methods such as the finite difference method (FDM)[7–10] and the finite element method (FEM) [11–13] have been utilized. Using these efficient thermo-chemical models, process optimization studies [14–16] as well as reliability analysis [17] have been performed. In [18], numerical modelling strategies for the thermo-chemical simulation of the pultrusion were investigated by the authors where the steady state approach was found to be computationally faster than the transient approach. In addition to these thermo-chemical studies in the literature, state-of-the-art models have recently been proposed by the authors for the thermo-chemical-mechanical analysis of the pultrusion [19] in which the thermo-mechanical aspects including the evolution of the process induced stresses and distortions in the transverse direction together with the mechanical properties were addressed. In this numerical model, a three dimensional (3D) transient thermo-chemical model is sequentially coupled with a 2D quasi-static plane strain mechanical model for the pultrusion process of a unidirectional (UD) fiber reinforced profile by using the FEM. The cure hardening instantaneous linear elastic (CHILE) approach [20, 21] was utilized for the resin modulus development. The proposed 3D/2D approach, which was found to be computationally efficient, provides an increased understanding of the process by evaluating the development of the stresses and distortions as well as the mechanical properties during processing. In [22], an integrated modelling of the pultrusion process of a NACA0018 blade profile was carried out by the authors using the proposed 3D/2D mechanical analysis in [19]. The calculated residual stresses were transferred to the subsequent bending simulation of the pultruded blade profile and the internal stress distribution was evaluated taking the process induced residual stresses into account.

3D thermo-chemical-mechanical analysis of the pultrusion process has not been considered in literature up to now. A novel 3D numerical simulation tool embracing the mechanical

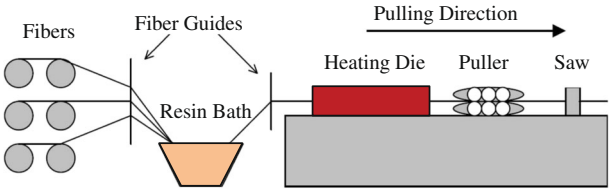

Fig. 1 Schematic view of a pultrusion process

aspects of the pultrusion process is hence being developed in the present work. The temperature and degree of cure distributions at steady state are first calculated using the 3D transient thermo-chemical analysis of a pultruded square product. Afterwards, these profiles are mapped to the 2D and 3D quasi-static mechanical models. The already developed 2D plane strain mechanical model in [19] is further improved using generalized plane strain elements. Moreover, 3D quadratic brick elements are used for the 3D model for the calculation of the process induced longitudinal stresses as well as transverse stresses. In the 3D mechanical model, instead of the cross section of the part which is used in the 2D mechanical model (see Fig. 3 [19]), the entire 3D part is assumed to move along the pulling direction of the process while tracking the corresponding temperature and degree of cure profiles calculated in the 3D thermo-chemical simulation (see Fig. 4). Using these three different mechanical models (i.e. 2D plane strain, 2D generalized plane strain and 3D models), the evolution of the transient stresses and distortions are captured and the obtained results are compared with each other. The general purpose finite element software package ABAQUS [23] is utilized. The CHILE approach, which is a valid pseudo-viscoelastic approximation of the linear viscoelasticity [24], is considered for the resin modulus evolution as in [19].

2 Numerical Implementation

2.1 Thermo-Chemical Model

In the thermo-chemical analysis, the energy equations are solved in 3D space for the UD pultruded part (Eq. 1) and for the die block (Eq. 2). Here, x_3 is the pulling (axial or longitudinal) direction; x_1 and x_2 are the transverse directions.

$$\rho_c Cp_c \left(\frac{\partial T}{\partial t} + u \frac{\partial T}{\partial x_3} \right) = k_{x_1,c} \frac{\partial^2 T}{\partial x_1^2} + k_{x_2,c} \frac{\partial^2 T}{\partial x_2^2} + k_{x_3,c} \frac{\partial^2 T}{\partial x_3^2} + q \tag{1}$$

$$\rho_d Cp_d \left(\frac{\partial T}{\partial t} \right) = k_{x_1,d} \frac{\partial^2 T}{\partial x_1^2} + k_{x_2,d} \frac{\partial^2 T}{\partial x_2^2} + k_{x_3,d} \frac{\partial^2 T}{\partial x_3^2} \tag{2}$$

where T is the temperature, t is the time, u is the pulling speed, ρ is the density, Cp is the specific heat and k_{x_1}, k_{x_2} and k_{x_3} are the thermal conductivities along x_1-, x_2- and x_3-directions, respectively. The subscripts c and d correspond to composite and die, respectively. Lumped material properties are used and assumed to be constant throughout the process [19]. The source term q in Eq. 1 is related to the internal heat generation due to the exothermic resin reaction of the thermosetting epoxy resin and expressed as [11]:

$$q = (1 - V_f) \rho_r H_{tr} R_r(\alpha, T) \tag{3}$$

where H_{tr} is the total heat of reaction for the epoxy during the exothermic reaction, ρ_r is the resin density, V_f is the fiber volume fraction, α is the degree of cure, and $R_r(\alpha, T)$ is the reaction of cure which can also be defined as the rate of α. H_{tr} is calculated from the

areas under the heat flow rate as a function of time obtained from the differential scanning calorimetry (DSC) tests. In literature, several kinetic models have been proposed and analyzed to describe the resin curing reactivity [25, 26]. In the present work, the well known modified n^{th}-order kinetic model is utilized in which the shift from a kinetics-dominated to a diffusion-dominated resin reaction near the point of vitrification (i.e. transition from rubbery to glassy state) is taken into account by a diffusion factor $f(\alpha, T)$ [19, 20, 27]. The corresponding expression is given as:

$$R_r(\alpha, T) = \frac{d\alpha}{dt} = K_o \exp\left(-\frac{E}{RT}\right)(1-\alpha)^n \cdot f(\alpha, T) \tag{4}$$

and

$$f(\alpha, T) = \frac{1}{1 + \exp\left[C(\alpha - (\alpha_{C0} + \alpha_{CT} T))\right]} \tag{5}$$

where K_o is the pre-exponential constant, E is the activation energy, R is the universal gas constant and n is the order of reaction (kinetic exponent). C is a diffusion constant, α_{C0} is the critical degree of cure at $T = 0$ K and α_{CT} is a constant for the increase in critical α with T [20]. K_o, E, and n can be obtained by a curve fitting procedure applied to the experimental data evaluated using the DSC tests [9].

The transient time integration scheme for the rate of the degree of cure can be derived by using the *chain rule*. Using this, the rate of the degree of cure can be expressed as:

$$\frac{d\alpha}{dt} = \frac{\partial \alpha}{\partial t} + \frac{\partial \alpha}{\partial x_3}\frac{dx_3}{dt} = \frac{\partial \alpha}{\partial t} + u\frac{\partial \alpha}{\partial x_3} \tag{6}$$

and from Eq. 6, the relation of the resin kinetics equation can be expressed as:

$$\frac{\partial \alpha}{\partial t} = R_r(\alpha, T) - u\frac{\partial \alpha}{\partial x_3} \tag{7}$$

where it is the expression in Eq. 7 used in the 3D transient thermo-chemical model. The equations presented above have been solved in a 3D domain by means of in-house developed routines implemented into the commercial software package ABAQUS.

2.2 Thermo-chemical-mechanical Model

The temperature- and cure-dependent instantaneous resin modulus is defined as suggested in the CHILE approach [20]. The corresponding relation is given as:

$$E_r = \begin{cases} E_r^0 & T^* \le T_{C1} \\ E_r^0 + \dfrac{T^* - T_{C1}}{T_{C2} - T_{C1}}(E_r^\infty - E_r^0) & for\ T_{C1} < T^* < T_{C2} \\ E_r^\infty & T_{C2} \le T^* \end{cases} \tag{8}$$

where E_r^0 and E_r^∞ are the initial (i.e. uncured) and fully cured resin moduli, respectively. T_{C1} and T_{C2} are the critical temperatures at the onset and completion of the glass transition, respectively, T^* represents the difference between the glass transition temperature (T_g) and the instantaneous resin temperature, i.e. $T^* = T_g - T$ [20]. The evolution of the T_g with the degree of cure is modelled by the Di Benedetto equation [28] and expressed as:

$$\frac{T_g - T_{g0}}{T_{g\infty} - T_{g0}} = \frac{\lambda \alpha}{1 - (1-\lambda)\alpha} \tag{9}$$

where T_{g0} and $T_{g\infty}$ are the glass transition temperatures of uncured and fully cured resin, respectively, λ is a constant used as fitting parameter.

The instantaneous resin elastic modulus (E_r) is used in the calculation of the effective mechanical properties as well as the thermal and shrinkage strains of the composite part as reported in [19].For this purpose, the self consistent field micromechanics (SCFM) approach is employed which is a well known and documented method in the literature to predict the effective mechanical properties of the UD composites [2, 19].

An incremental linear elastic approach is implemented utilizing user defined subroutines in ABAQUS for the calculation of the residual stresses and distortions in 2D and 3D mechanical analyses of the pultrusion process. As aforementioned, quadratic plane strain and generalized plane strain elements for the 2D analysis and brick elements for the 3D analysis are employed. The incremental total strain tensor ($\dot{\varepsilon}_{ij}^{tot}$) is composed of the incremental mechanical strain ($\dot{\varepsilon}_{ij}^{mech}$), thermal strain ($\dot{\varepsilon}_{ij}^{th}$) and chemical strain ($\dot{\varepsilon}_{ij}^{ch}$) tensors and expressed as:

$$\dot{\varepsilon}_{ij}^{tot} = \dot{\varepsilon}_{ij}^{mech} + \dot{\varepsilon}_{ij}^{th} + \dot{\varepsilon}_{ij}^{ch} \tag{10}$$

The incremental stress tensor $\dot{\sigma}_{ij}$ is then calculated using the material Jacobian matrix (**J**) based on the incremental mechanical strain tensor $\dot{\varepsilon}_{ij}^{mech}$ [23] and the corresponding expression is given as:

$$\dot{\sigma}_{ij} = \mathbf{J}\dot{\varepsilon}_{ij}^{mech} \tag{11}$$

The details of the relation between the stress and strain tensors used in the present 2D finite element implementation can be found in [19]. The extension of the corresponding relation for the 3D mechanical analysis is presented in Eq. 12.

$$\begin{pmatrix} \dot{\sigma}_{11} \\ \dot{\sigma}_{22} \\ \dot{\sigma}_{33} \\ \dot{\tau}_{12} \\ \dot{\tau}_{13} \\ \dot{\tau}_{23} \end{pmatrix} = \begin{bmatrix} J_{11} & J_{12} & J_{13} & 0 & 0 & 0 \\ J_{21} & J_{22} & J_{23} & 0 & 0 & 0 \\ J_{31} & J_{32} & J_{33} & 0 & 0 & 0 \\ 0 & 0 & 0 & J_{44} & 0 & 0 \\ 0 & 0 & 0 & 0 & J_{55} & 0 \\ 0 & 0 & 0 & 0 & 0 & J_{66} \end{bmatrix} \begin{pmatrix} \dot{\varepsilon}_{11} \\ \dot{\varepsilon}_{22} \\ \dot{\varepsilon}_{33} \\ \dot{\gamma}_{12} \\ \dot{\gamma}_{13} \\ \dot{\gamma}_{23} \end{pmatrix}^{mech} \tag{12}$$

where $\dot{\tau}_{ij}$ is the incremental shear stress tensor, $\dot{\gamma}_{ij}$ is the incremental shear strain tensor and J_{ij}'s are the elements of the material Jacobian matrix (**J**) [23].

3 Model Description

3.1 Thermo-Chemical Analysis

A 3D thermo-chemical analysis for the pultrusion of a relatively thick (25.4 mm) square profile is carried out in a Eulerian frame. The pultrusion model is taken from similar set-ups available in the literature [9, 11, 19]. A glass/epoxy is considered for the pultruded product in which the fiber reinforcement orientation is UD along the pulling direction and chrome steel is used for the die. Material properties and the resin kinetic parameters are listed in Table 1 and Table 2, respectively [9, 19]. Only a quarter of the pultrusion domain, seen in Fig. 2, is modelled due to symmetry. Three heating zones having prescribed set temperatures of 171-188-188°C (see Fig. 2) are defined and the spacing between these zones is defined as 15 mm [9]. The details of the cross section are also shown in Fig. 2. Perfect thermal contact is assumed at the die-part interface as in [11, 19]. Initially ($t = 0$), the temperature of all nodes are assigned to ambient temperature (27°C) and the degree of

Table 1 Material Properties used in the thermo-chemical simulation of the pultrusion process [9]

Material	ρ [kg/m^3]	Cp [J/kg K]	k_{x_3} [W/m K]	k_{x_1}, k_{x_2} [W/m K]	V_f
Epoxy resin	1260	1255	0.21	0.21	36.1%
Glass fiber	2560	670	11.4	1.04	63.9%
Steel die	7833	460	40	40	-

Table 2 Epoxy resin kinetic parameters [9, 19]

H_{tr}[kJ/kg]	K_0[1/s]	E[kJ/mol]	n	C	α_{C0}	α_{CT} [1/K]
324	192,000	60	1.69	30	-1.5	0.0055

cure of all composite nodes are assigned to 0. For $t > 0$, the temperature of the composite nodes at the die inlet are set to the resin bath temperature 30 °C and the degree of cure to 0, respectively. At the symmetry surfaces adiabatic boundaries are defined in which no heat flow is allowed across the boundaries. The remaining exterior surfaces of the die are exposed to ambient temperature with a convective heat transfer coefficient of 10 W/(m^2 K) except for the surfaces located at the heating regions. Similarly, at the post die region, convective boundaries are defined for the exterior surfaces of the pultruded square profile. The heat transfer coefficient utilized in the thermo-chemical analysis is an overall value which actually accounts for both convective and radiation heat transfer during the post-die cooling of the part. The choice of this value (within the realistic range) is not crucial for the results of the model. The length of the post die region (L_{conv}) is determined to be 13.7 m for cooling down to the ambient temperature after die exit. To reach steady state, the convergence limits are defined as the maximum temperature and cure degree difference between the new time step and the old time step and these are set to 0.001 °C and 0.0001, respectively.

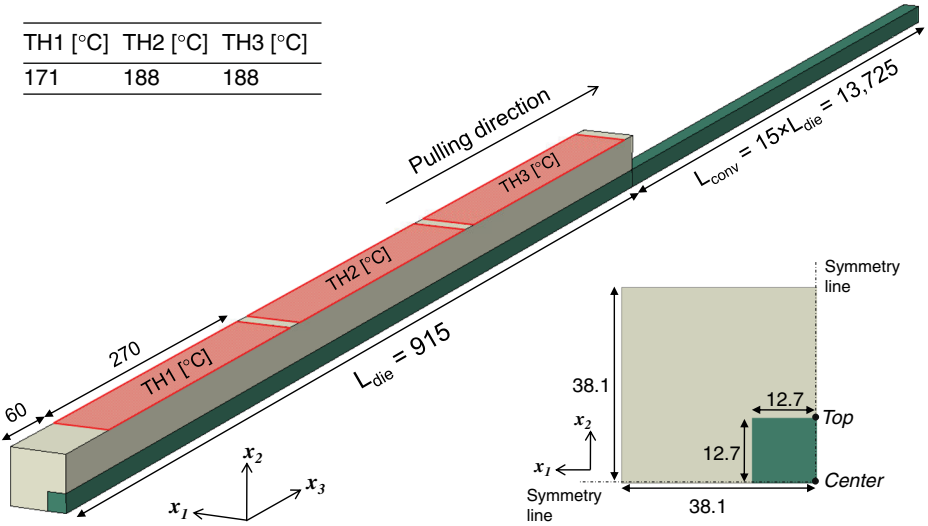

Fig. 2 Schematic view of the pultrusion domain for the pultruded square beam. All dimensions are in mm

3.2 Thermo-Chemical-Mechanical Analysis: 2D Approach

In the 2D approach, the 3D thermo-chemical model defined in Section 3.1 is coupled with a 2D quasi-static mechanical model. Quadratic plane strain and generalized plane strain elements are utilized separately for a comparison analysis of the process induced stress and distortion evolutions. In this 2D mechanical model, the cross section of the composite is moved through the pulling direction during the process (Lagrangian frame) meanwhile tracking the corresponding temperature and degree of cure profiles already calculated in the 3D thermo-chemical analysis (Eulerian frame). Since the length of the pultruded profile is generally much higher than the cross sectional dimensions, the plain strain assumption is convenient for the analysis of the pultrusion process [19]. For the mechanical analysis, the die is assumed to be rigid and therefore rigid body surfaces are added at the die-part interface instead of including the meshing for the whole die as was done in the thermo-chemical analysis. Between the rigid surfaces and the composite part, a mechanical contact formulation is defined which allows separation due to resin shrinkage at the interface and restricts any expansion of the composite beyond the tool interface. The friction force at the contact surfaces is assumed to be zero (sliding condition). A generic view of the plane strain model including the rigid surfaces and the mechanical boundary conditions (BCs) are shown in Fig. 3. The resin parameters used in the CHILE approach for the elastic modulus development are listed in Table 3.

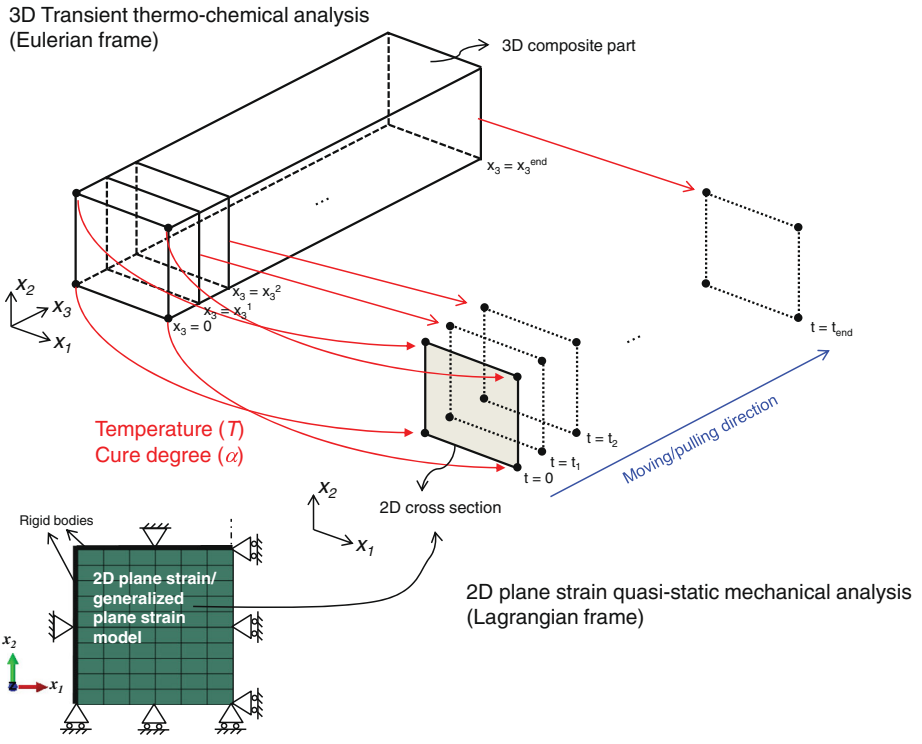

Fig. 3 Representation of the coupling of the 3D Eulerian thermo-chemical model with the 2D Langrangian plain-strain/generalized-plane-strain mechanical model including the rigid body surfaces and the mechanical BCs

Table 3 Epoxy resin parameters used in the CHILE approach[19, 20]

T_{C1}[°C]	T_{C2}[°C]	E_r^0[MPa]	E_r^∞[MPa]	λ	T_{g0} [°C]	$T_{g\infty}$ [°C]
-45.7	12	3.447	3.447e3	0.4	0	195

3.3 Thermo-Chemical-Mechanical Analysis: 3D Approach

In 3D approach, the development of the process induced stresses and distortions are predicted using a 3D quasi-static mechanical model. In this model, the entire 3D composite part defined in Section 3.1 is assumed to be advanced through the pulling direction while tracking the mapped thermal and cure history. In other words, a 3D Eulerian thermo-chemical model is coupled with a 3D quasi-static Lagrangian mechanical model (see Fig. 4). As similar to the 2D approach, the die surfaces are modelled as rigid surfaces with a similar mechanical contact formulation defined in Section 3.2. Mechanical symmetry BCs are applied at the symmetry surface in the x_1- and x_2-directions. There is no applied mechanical BC in the x_3-direction, i.e. the part can freely move or rotate in the x_3-direction. The corresponding process induced stresses and distortions are calculated based on the temperature and the cure distributions together with the corresponding glass transition temperature (T_g) of the composite part. 3D quadratic brick elements are used in the 3D mechanical analysis. The effective mechanical properties of the pultruded part are calculated using the SCFM approach as aforementioned.

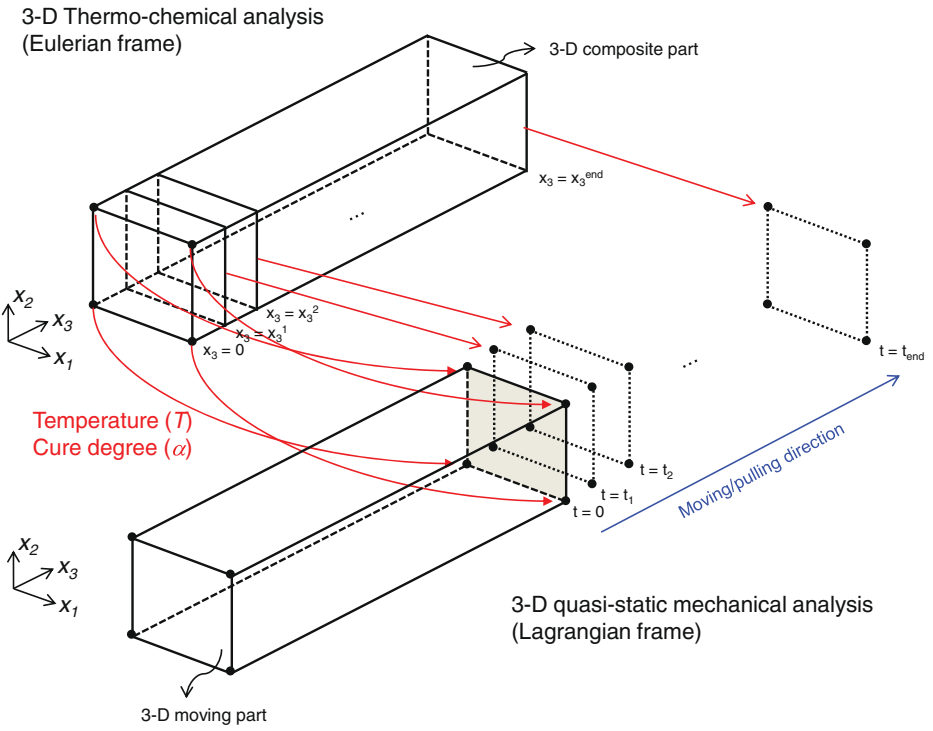

Fig. 4 Representation of the coupling of the 3D thermo-chemical model with the 3D mechanical model

4 Results and Discussions

The temperature and the degree of cure profiles together with T_g at steady state are first calculated in the 3D transient thermo-chemical analysis for the pultrusion of the square beam defined in Section 3.1. These results are depicted in Fig. 5 and Fig. 6. When the pultruded part enters the heating die, it follows these steady state profiles since pultrusion is a continuous process. The pulling speed is set to 20 cm/min [9, 19]. Here, "*top*" and "*center*" denote the top line and the center line through the whole length of the part, respectively, as also shown in Fig. 2. It is seen that non-uniform temperature (Fig. 5) and degree of cure (Fig. 6) distributions are obtained. The *top* cures earlier than the *center* since it is closer to the die having heaters on top of it (Fig. 2). The maximum temperature at the *center* is predicted as approximately 217°C which is higher than the heater temperature (i.e. 188°C) due to the exothermic internal heat generation of the epoxy resin. T_g crosses the composite temperature of around 173°C for the *top* and 182°C for the *center* at approximately 1.6 m and 1.8 m from die inlet, respectively [19]. It is seen from Fig. 6 that at the post die region ($x_3 > 0.915$ m) the degree of cure is increased slightly which indicates that the curing still takes place after the die exit. This fact was also observed in [8]. The degree of cure at the *center* is calculated to be approximately 0.97 at the end of the process (i.e. $x_3 \cong 14.6$ m).

The obtained temperature and degree of cure distributions together with T_g are mapped to the 2D and 3D quasi-static mechanical analyses as described in Section 3.2 and Section 3.3. In order to reflect the 3D thermo-chemical-mechanical behaviour of the process more precisely, the mid section of the composite part is considered since the pultrusion is a continuous process, i.e. there is always existing material inside the heating die during the process. The mid section is far away from the end boundaries as seen in Fig. 7 in which a schematic view of the movement of the 3D part in the pulling direction is also depicted. It should be noted that the tracking of the mid section starts at $x_3 \cong -7.3$ m and ends at $x_3 \cong 7.3$ m (end of the process). At $x_3 = 0$ m, the mid section enters the heating die. The corresponding mapped temperature and degree of cure distributions at the mid section are

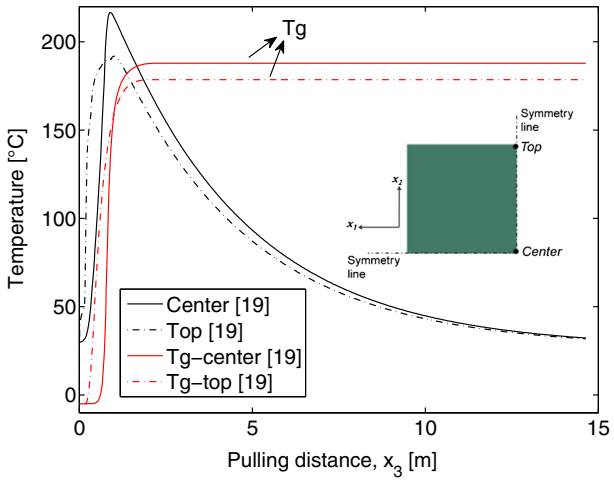

Fig. 5 The temperature and T_g distributions for *center* and *top* at the steady state (3D transient thermo-chemical approach)

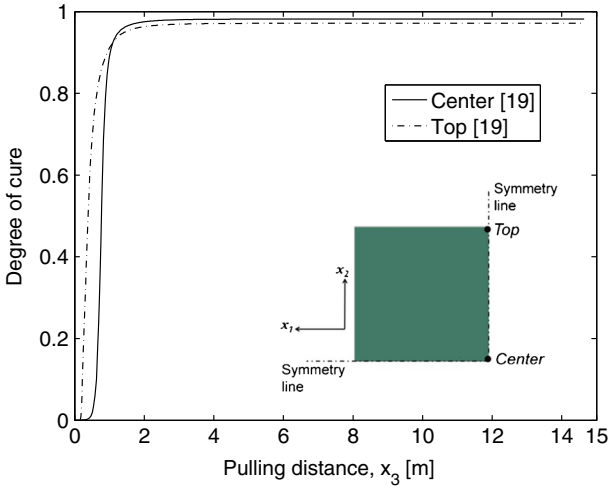

Fig. 6 The degree of cure profiles for *center* and *top* at the steady state (3D transient thermo-chemical approach)

shown in Fig. 8 and Fig. 9, respectively. It is seen that until the mid section enters the heating die, it is assumed that the temperature remains constant as the resin bath temperature of 30°C and the material remains uncured, i.e. $\alpha = 0$. After entering the heating die, the mid section starts tracking the calculated thermal and cure history. This shows that the calculation domain for the 3D mechanical analysis is between $x_3 \cong -7.3$ m and $x_3 \cong 7.3$ m, on the other hand this is between $x_3 = 0$ m and $x_3 \cong 14.6$ m for the 2D mechanical analysis.

The evolution of the transient stresses are obtained using the 2D plane strain, generalized plane strain and 3D quadratic elements in ABAQUS. These results are depicted in Fig. 10

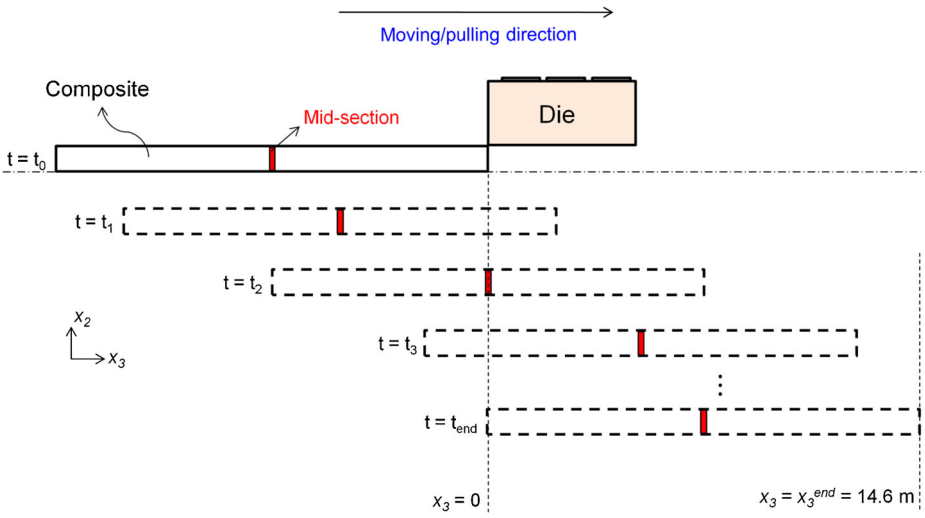

Fig. 7 Schematic view of the movement of the 3D part in the pulling direction and the positioning of the mid section. The sizes of the die and the part are not scaled

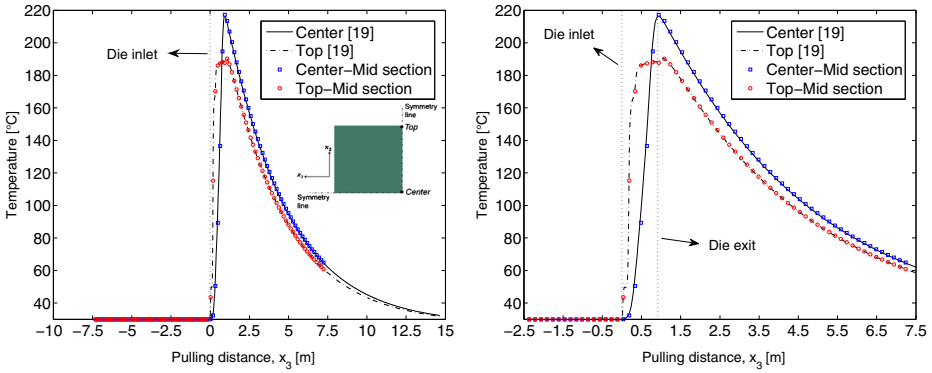

Fig. 8 Mapped temperature distributions for *center* and *top* at the mid section of the 3D part (*left*). The corresponding zoomed plot of the temperature profiles (*right*) for the axial distance between -2.5 m and 7.5 m

and Fig. 11 for *center* and *top*, respectively. Here, S11, S22 and S33 are the normal stresses in the x_1-direction (horizontal, transverse), the x_2-direction (vertical, transverse) and the x_3-direction (longitudinal), respectively. It is seen that the transverse normal stresses are found to be almost similar using both 2D and 3D approaches in terms of magnitude and evolution trend as compared with published data [19]. It is obvious that the 3D mechanical model is a more advanced and realistic numerical tool as compared to 2D models. Bearing this in mind, the plane strain assumption for the mechanical analysis of the pultrusion process gives accurate results and is a convenient way of modelling for the prediction of transverse stresses. For the 3D mechanical analysis, it is seen that until the mid section enters the die, there is almost no transverse stresses, i.e. S11 and S22 are zero before the die inlet. This shows that the already pulled material (e.g. the portion inside the heating die) has almost no effect on the stress development at the mid section before entering the die. Inside the die, the stress levels are relatively small because the matrix material has not enough stiffness

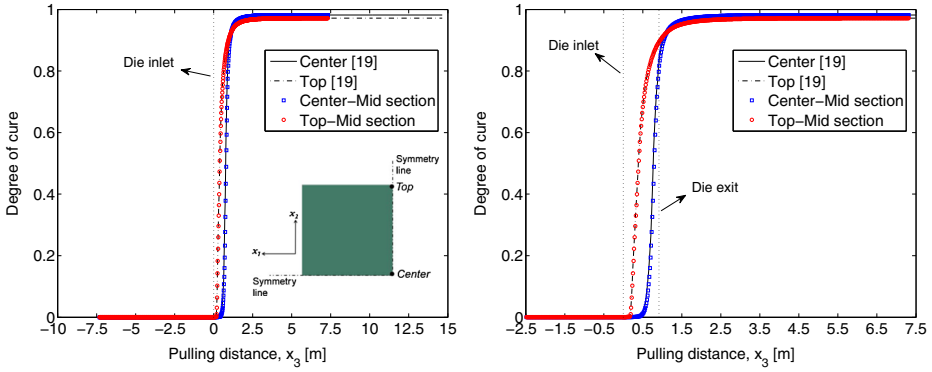

Fig. 9 Mapped degree of cure distributions for *center* and *top* at the mid section of the 3D part (*left*). The corresponding zoomed plot of the degree of cure profiles (*right*) for the axial distance between -2.5 m and 7.5 m

to build up the stresses. The outer regions closest to the die cure first which make them constrained by the inner region during shrinkage. Due to this, a residual compression is found in these regions and tension prevails for the inner regions at the end of the process upholding the self static equilibrium.

Regarding the longitudinal stress development (S33 for *center* in Fig. 10 and for *top* in Fig. 11) in the pulling or fiber direction, a different mechanical behaviour is obtained as compared to the development in the transverse directions (S11 and S22). It is seen that unrealistic and overestimated transient S33 values are obtained using the plane strain elements. On the other hand "more" realistic stress values are calculated using the generalized plane strain elements since out-of-plane strain is now allowed to take place within certain restrictions. Therefore, the resulting S33 values obtained by using the generalized plane strain elements are much closer to the values in the 3D mechanical analysis. Although the matrix material is in a liquid state before entering the die (the degree of cure is zero) for the 3D mechanical analysis, a non-zero S33 (value of approximately 2 MPa) is found to exist at the mid section (*center*) while entering the die as seen in Fig. 10d. From modelling point of view, this is due to the stress gradient through the thickness in combination with a low

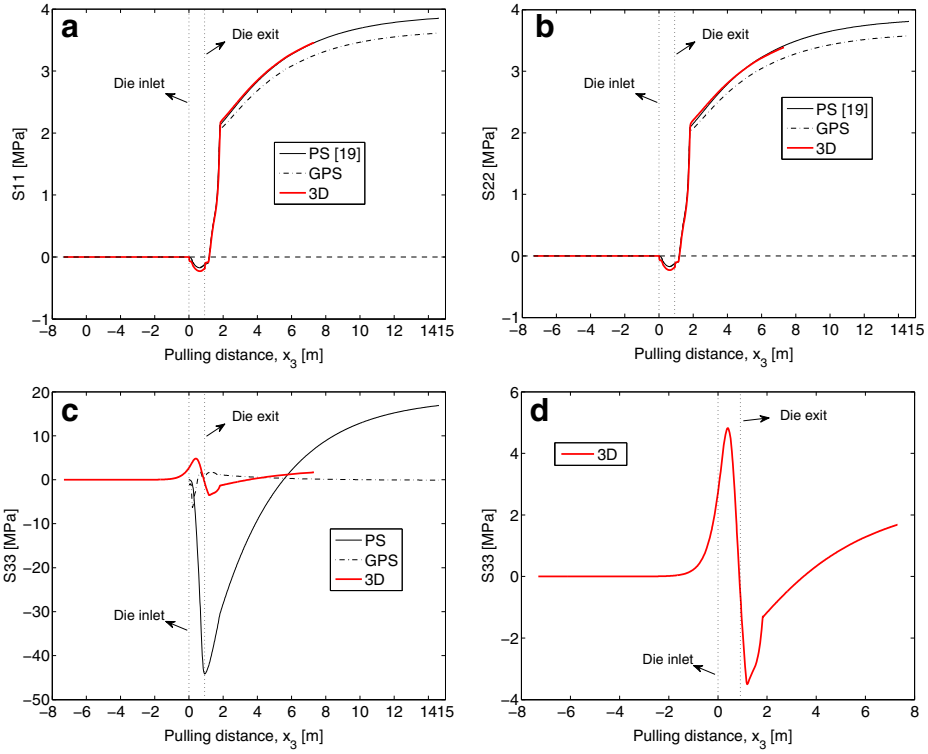

Fig. 10 The transient stress evolutions at *center* (S11 (a), S22 (b) and S33 (c)) which are calculated using the plane strain (PS), generalized plane strain (GPS) and 3D quadratic brick elements. The zoomed plot of S33 for 3D elements are depicted in (d)

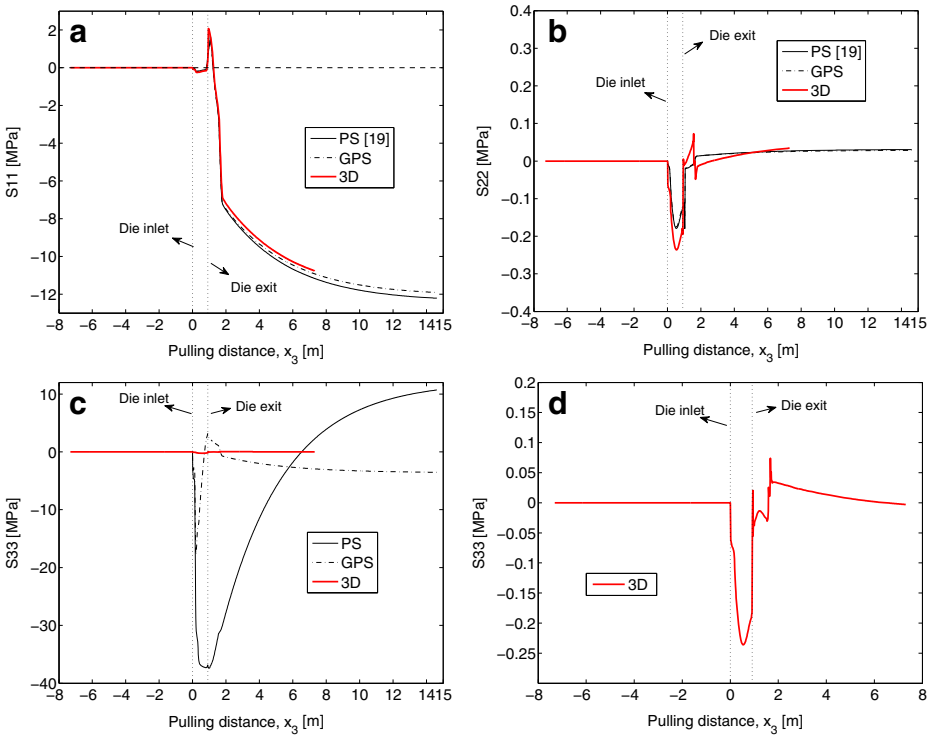

Fig. 11 The transient stress evolutions at *top* (S11 (a), S22 (b) and S33 (c)) which are calculated using the plane strain (PS), generalized plane strain (GPS) and 3D quadratic brick elements. The zoomed plot of S33 for 3D elements are depicted in (d)

shear modulus at the liquid state. Nevertheless, it will not appear in practice and the region before die is out of interest in terms of the mechanical variations in the processing material. As mentioned before, this 3D effect is not pronounced in the transverse directions. The longitudinal stress levels (S33) calculated using the generalized plane strain and 3D elements are found to be relatively small as compared to S11 and S22 since the longitudinal component of the process induced strain is smaller than the transverse component (see Fig. 12 for the process induced strain development at *center*). The reason for that is the constraining fiber stiffness in the pulling direction which was also investigated in [2].

The corresponding contour plots of S11, S22 and S33 at the end of the process are seen in Fig. 13 (plane strain solution), Fig. 14 (generalized plane strain solution) and Fig. 15 (3D solution). The stress distributions in the transverse directions (i.e. S11 and S22) over the cross section of the part have almost the same pattern for these three different types of analysis. As expected, the S11 distribution is almost symmetric with the S22 distribution with respect to the diagonal of the pultruded part, since all the mechanical boundary conditions are the same. The generalized plane strain results (Fig. 14) and the 3D results (Fig. 15) have the similar distribution trend for the S33 distribution, such that tension and compression stresses are found to prevail in the pulling direction. On the other hand, the plane

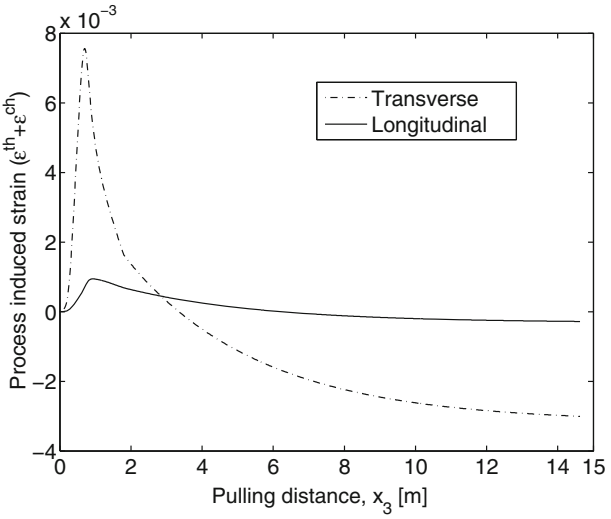

Fig. 12 The process induced strain, which is the summation of the thermal strain (ε^{th}) and the chemical shrinkage strain (ε^{ch}), for *center* in the transverse and longitudinal direction

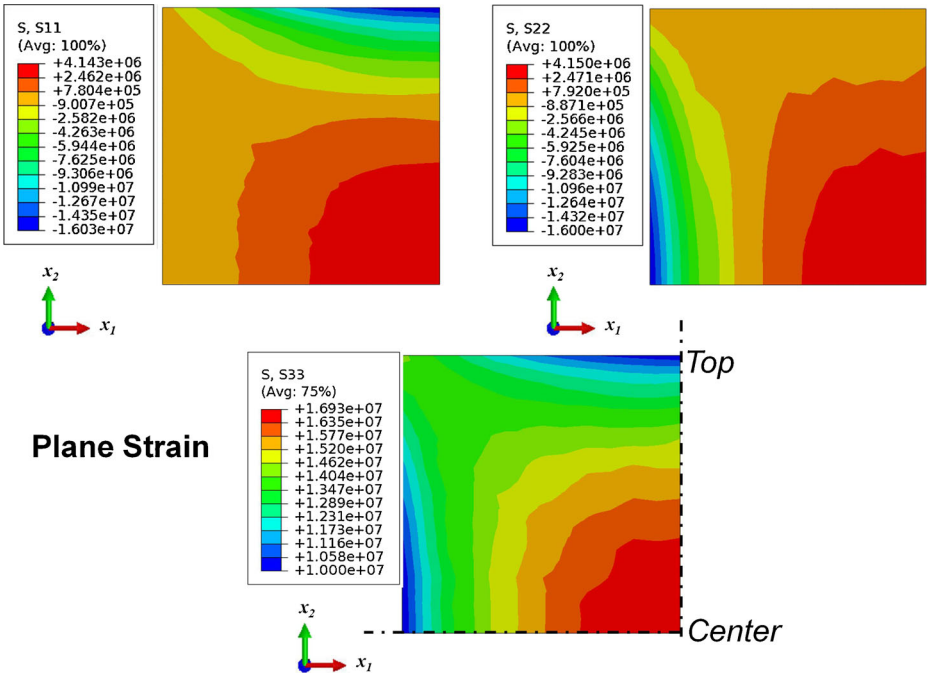

Fig. 13 Undeformed contour plots of the normal stresses S11, S22 and S33 calculated using the plane strain elements at the end of the process ($x_3 \cong 14.6$ m). All units are in Pa

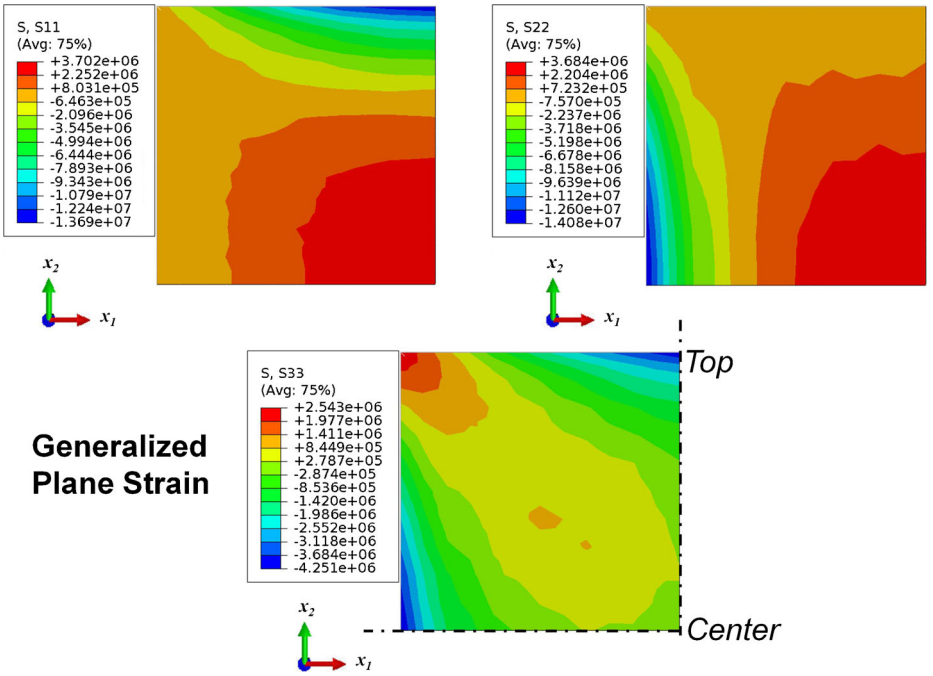

Fig. 14 Undeformed contour plots of the normal stresses S11, S22 and S33 calculated using the generalized plane strain elements at the end of the process ($x_3 \cong 14.6$ m). All units are in Pa

strain solution predicts unrealistic S33 values such that the whole cross section is under tension showing that the self static equilibrium in the longitudinal direction is not fulfilled as expected. The reason for this is that there is no strain in the longitudinal direction for the plane strain assumption. This may not be a valid assumption for the calculation of the S33 since there is an existing strain in the pulling direction.

The calculated maximum tension and compression stresses at the end of the process are given in Table 4. It is seen that the lowest stress levels are obtained for the 3D mechanical solution which is also intuitively expected. The maximum tension stress level is found to be approximately between 3-4 MPa and the maximum compression level is approximately between 12-16 MPa for S11 and S22. For S33, the levels are approximately between 1.7-2.5 MPa and 3.65-4.25 MPa, respectively, without considering the plane strain solution since it is overestimating S33.

The evolution of the displacement profile is also predicted using the devised numerical simulation tools for the *top* in the x_2-direction (U2). The results are depicted in Fig. 16. It is found that there is a good match between the U2 evolutions obtained using the three different element types. It should be noted that the initial pressure condition of the part before entering the heating die is not taken into account which may affect the stress and displacement field.

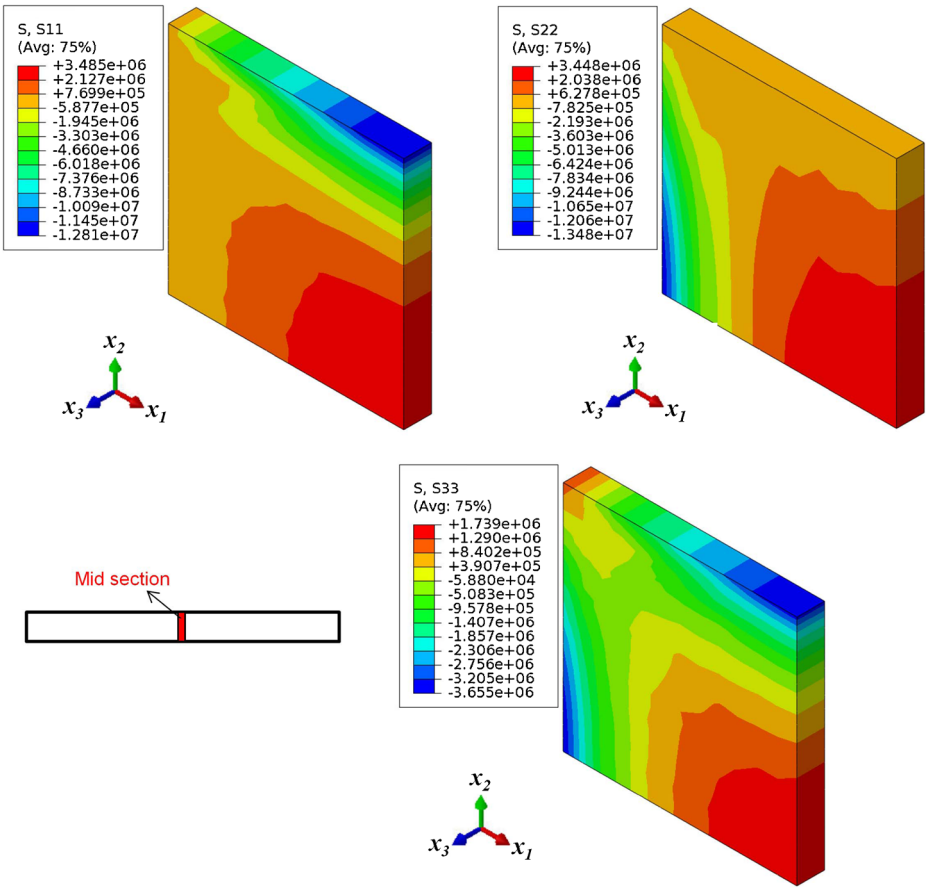

Fig. 15 Undeformed contour plots of the normal stresses S11, S22 and S33 for the mid section (see Fig. 7) calculated using the 3D elements at the end of the process ($x_3 \cong 7.3$ m). All units are in Pa

Table 4 The maximum tension and compression stresses predicted at the cross section of the pultruded product using the plane strain (PS), generalized plane strain (GPS) and the 3D elements.

	S11 [MPa]	S22 [MPa]	S33 [MPa]
Max. tension	4.14 (PS)	4.15 (PS)	16.93 (PS)
	3.70 (GPS)	3.68 (GPS)	2.54 (GPS)
	3.48 (3D)	3.44 (3D)	1.74 (3D)
Max. compression	16.03 (PS)	16.00 (PS)	- (PS)
	13.69 (GPS)	14.00 (GPS)	4.25 (GPS)
	12.81 (3D)	13.48 (3D)	3.65 (3D)

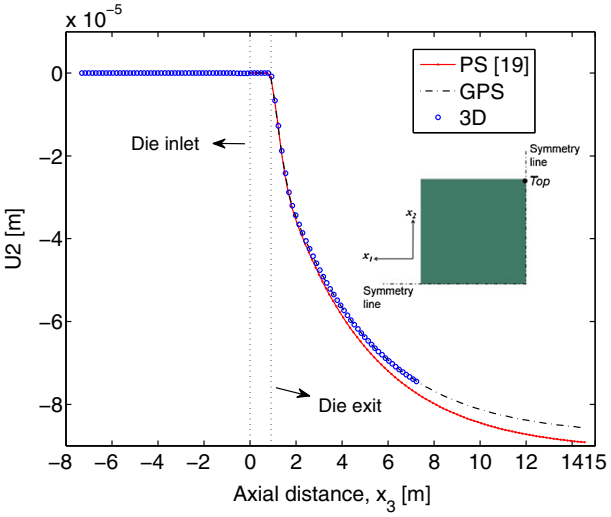

Fig. 16 Displacement evolution for *top* in the x_2-direction (U2) calculated using the plane strain (PS), generalized plane strain (GPS) and 3D elements (mid section for the 3D model)

5 Conclusions

In the present work, the 2D quasi-static plane strain mechanical model developed by the authors for the pultrusion process is further improved using the generalized plane strain elements. In addition, 3D quadratic brick elements are also utilized for the 3D thermo-chemical-mechanical model for the calculation of the longitudinal stresses which has not been considered up to now in the field of numerical modelling of the pultrusion process. The temperature and degree of cure distributions at steady state are first calculated using a 3D transient thermo-chemical analysis. Afterwards, these profiles are mapped to the 2D and 3D quasi-static mechanical models. Using these three different mechanical models (i.e. 2D plane strain, 2D generalized plane strain and 3D models), the development of the process induced stresses and distortions are predicted for the pultrusion of a UD glass/epoxy square profile. The obtained results are compared with each other. The main outcomes are summarized as follows:

i) It is found that there is a good agreement between the calculated transverse stress evolutions (S11 and S22) together with the transverse displacement profiles (U2) using the 2D and 3D mechanical models. This shows that the plane strain assumption is a convenient and fast way of predicting the transverse stresses and displacements.

ii) For the calculation of the longitudinal stresses (S33), generalized plane strain and 3D elements predict "more" realistic stress values as compared to the plane strain elements in which overestimated S33 values are obtained.

iii) The predicted stress level for S33 is found to be lower than the S11 and S22 since the longitudinal component of the process induced strain is smaller than the transverse component.

iv) Lower stress values are obtained in the 3D mechanical analysis as compared with the 2D analyses which is intuitively expected.

The proposed 3D/3D thermo-chemical-mechanical model is found to be more suitable for advanced modelling of the pultrusion process, e.g. taking the effect of the frictional force inside the heating die on the longitudinal process induced stress levels into account. On the other hand, the 2D generalized plane strain mechanical model is found to be computationally fast as compared with the 3D model and is therefore more efficient and useful for internal stress investigation in the transverse directions of the pultruded products, e.g. the transverse residual stresses at the web-flange junctions of pultruded I-beam profiles or transverse warpage in pultruded hollow rectangular profiles.

Acknowledgments This work is a part of the DeepWind project which has been granted by the European Commission (EC) under the FP7 program platform Future Emerging Technology.

References

1. Wisnom, M.R., Gigliotti, M., Ersoy, N., Campbell, M., Potter, K.D.: Mechanisms generating residual stresses and distortion during manufacture of polymermatrix composite structures, Vol. 37, pp. 522–529 (2006)
2. Bogetti, T.A., Gillespie, J.W.: Process-induced stress and deformation in thick-section thermoset composite laminates. J. Compos. Mater. **26**(5), 626–660 (1992)
3. Ersoy, N., Garstka, T., Potter, K., Wisnom, M.R., Porter, D., Stringer, G.: Modelling of the spring-in phenomenon in curved parts made of a thermosetting composite. Compos. Part A **41**, 410–418 (2010)
4. White, S.R., Hahn HT: Process modeling of composite materials:Residual stress development during cure. Part I. Model formulation. J. Compos. Mater. **26**(16), 2402–2422 (1992a)
5. White, S.R., Hahn HT: Process Modeling of Composite Materials:Residual Stress Development during Cure. Part II. Experimental Validation. J. Compos. Mater. **26**(16), 2423–2453 (1992b)
6. Nielsen, M.W., Schmidt, J.W., Hattel, J.H., Andersen, T.L., Markussen, C.M.: In situ measurement using FBGs of process-induced strains during curing of thick glass/epoxy laminate plate: experimental results and numerical modelling. Wind energy 2012.
7. Baran, I., Tutum, C.C., Hattel, J.H.: The effect of thermal contact resistance on the thermosetting pultrusion process. Compos. Part B: Eng. **45**, 995–1000 (2013)
8. Valliappan, M., Roux, J.A., Vaughan, J.G., Arafat, E.S.: Die and post-die temperature and cure in graphite-epoxy composites. Compos. Part B-Eng. **27**, 1–9 (1996)
9. Chachad, Y.R., Roux, J.A., Vaughan, J.G., Arafat, E.: Three-dimensional characterization of pultruded fiberglass-epoxy composite materials. J. Reinf. Plast. Comp. **14**, 495–512 (1995)
10. Ding Z, Li S, Lee LJ.: Influence of heat transfer and curing on the quality of pultruded composites. ii: Modeling and simulation. Polym. Compos. **23**, 957–969 (2002)
11. Liu, X.L., Crouch, I.G., Lam, Y.C.: Simulation of heat transfer and cure in pultrusion with a general-purpose finite element package. Compos. Sci. Technol. **60**, 857–864 (2000)
12. Carlone, P., Palazzo, G.S., Pasquino, R.: Pultrusion manufacturing process development by computational modelling and methods. Math. Comput. Model. **44**, 701–709 (2006)
13. Suratno, B.R., Ye, L., Mai, Y.W.: Simulation of temperature and curing profiles in pultruded composite rods. Compos. Sci. Technol. **58**, 191–197 (1998)
14. Carlone, P., Palazzo, G.S.: Pultrusion manufacturing process development:Cure optimization by hybrid computational methods. Comput. Math. Appl. **53**, 1464–1471 (2007)
15. Baran, I., Tutum, C.C., Hattel, J.H.: Optimization of the thermosetting pultrusion process by using hybrid and mixed integer genetic algorithms. App. Compos. Mat. **20**, 449–463 (2012)
16. Tutum, C.C., Baran, I., Hattel, J.H.: Utilizing multiple objectives for the optimization of the pultrusion process. Key Eng. Mater. **554-557**, 2165–2174 (2013)
17. Baran, I., Tutum, C.C., Hattel, J.H.: Reliability estimation of the pultrusion process using the first-order reliability method (FORM). App. Compos. Mat. **20**, 639–653 (2012)
18. Baran, I., Hattel, J.H., Tutum, C.C.: Thermo-Chemical modelling strategies for the pultrusion process. App. Compos. Mat. (2013)
19. Baran, I., Tutum, C.C., Nielsen, M.W., Hattel, J.H.: Process induced residual stresses and distortions in pultrusion. Compos. Part B: Eng. **51**, 148–161 (2013)

20. Johnston A.: An integrated model of the development of process-induced deformation in autoclave processing of composites structures, Ph.D. thesis. The University of British Columbia, Vancouver (1997)
21. Nielsen MW: Predictions of process induced shape distortions and residual stresses in large fibre reinforced composite laminates, Ph.D. thesis, deparment of mech. Eng. Technical University of Denmark, Denmark (2012)
22. Baran, I., Tutum, C.C., Hattel, J.H.: The internal stress evaluation of the pultruded blades for a Darrieus wind turbine. Key Eng. Mater. **554-557**, 2127–2137 (2013)
23. ABAQUS 6.11 Reference Guide. Dassault Systems (2011)
24. Zobeiry, N., Rasekh, A., Vaziri, R., Poursartip, A.: Efficient modelling techniques for predicting processing residual stress and deformation in composite parts. Proceedings of the 14th international conference on composite materials ICCM-14, San Diego, United States of America (2003)
25. Kenny, J.M.: Determination of autocatalytic kinetic model parameters describing thermoset cure. J. Appl. Polym. Sci. **51**, 761–764 (1994)
26. Kessler, M.R., White, S.R.: Cure kinetics of the ring-Opening metathesis polymerization of dicyclopentadiene. J. Poly. Sci. Part A: Poly. Chem. **40**, 2373–2383 (2002)
27. Khoun, L.: Process-induced stresses deformations in woven composites manufactured by resin transfer moulding. Ph.D. Thesis,McGill University, Montreal (2009)
28. Khoun L, Centea T, Hubert P: Characterization methodology of thermoset resins for the processing of composite materials case study: CYCOM 890RTM epoxy resin. J. Compos. Mater. **44**, 1397415 (2010)